AGU PUBLICATIONS

JGR

Journal of Geophysical Research: Oceans

RESEARCH ARTICLE

10.1002/2014JC010227

Key Points:
- Methanol and acetone deposited from atmosphere to ocean in higher latitudes
- Total transfer velocity of methanol and acetone consistent with COARE model
- Comparing the transfer of two gases allows for estimation of k_a and k_w

Supporting Information:
- Summary of supporting information
- Intercomparison of wind speeds between two sonic anemometers
- Mean normalized cospectra of momentum and sensible heat

Correspondence to:
M. Yang,
miya@pml.ac.uk

Citation:
Yang, M., B. W. Blomquist, and P. D. Nightingale (2014), Air-sea exchange of methanol and acetone during HiWinGS: Estimation of air phase, water phase gas transfer velocities, *J. Geophys. Res. Oceans*, *119*, 7308–7323, doi:10.1002/2014JC010227.

Received 9 JUN 2014
Accepted 3 OCT 2014
Accepted article online 7 OCT 2014
Published online 29 OCT 2014

Air-sea exchange of methanol and acetone during HiWinGS: Estimation of air phase, water phase gas transfer velocities

Mingxi Yang[1], Byron W. Blomquist[2], and Philip D. Nightingale[1]

[1]Plymouth Marine Laboratory, Plymouth, UK, [2]Department of Oceanography, University of Hawaii, Honolulu, Hawaii, USA

Abstract The air-sea fluxes of methanol and acetone were measured concurrently using a proton-transfer-reaction mass spectrometer (PTR-MS) with the eddy covariance (EC) technique during the High Wind Gas Exchange Study (HiWinGS) in 2013. The seawater concentrations of these compounds were also measured twice daily with the same PTR-MS coupled to a membrane inlet. Dissolved concentrations near the surface ranged from 7 to 28 n*M* for methanol and from 3 to 9 n*M* for acetone. Both gases were consistently transported from the atmosphere to the ocean as a result of their low sea surface saturations. The largest influxes were observed in regions of high atmospheric concentrations and strong winds (up to 25 m s^{-1}). Comparison of the total air-sea transfer velocity of these two gases (K_a), along with the in situ sensible heat transfer rate, allows us to constrain the individual gas transfer velocity in the air phase (k_a) and water phase (k_w). Among existing parameterizations, the scaling of k_a from the COARE model is the most consistent with our observations. The k_w we estimated is comparable to the tangential (shear driven) transfer velocity previously determined from measurements of dimethyl sulfide. Lastly, we estimate the wet deposition of methanol and acetone in our study region and evaluate the lifetimes of these compounds in the surface ocean and lower atmosphere with respect to total (dry plus wet) atmospheric deposition.

1. Introduction

Oxygenated Volatile Organic Compounds (OVOCs) in the atmosphere influence the tropospheric oxidative capacity and global methane budget via the cycling of HO_x ($OH + HO_2$) and ozone [*Carpenter et al*., 2012]. In a model evaluation of observations at a tropical Atlantic site by *Read et al*. [2012], inclusion of OVOCs led to a 37–45% reduction in the OH radical concentration in the marine boundary layer compared to the no OVOC case. Here we focus on methanol and acetone—two of the most ubiquitous OVOCs. Second in abundance amongst organic gases in the global atmosphere after methane, methanol is a precursor to carbon monoxide [*Duncan et al*., 2007] and formaldehyde [*Millet et al*., 2006]. Acetone is a precursor to the pollutant peroxyacetyl nitrate (PAN) as well as a significant source of HO_x in the dry upper troposphere [*Singh et al*., 1995; *Neumaier et al*., 2014]. According to the synthesis by *Heald et al*. [2008], together methanol and acetone constituted ~40% of the total (nonmethane) observed organic carbon (gaseous and particulate) in the remote marine atmosphere.

Terrestrial plants produce substantial quantities of methanol and acetone; additional sources of these compounds include biomass and fossil fuel burning, industrial emissions, and atmospheric oxidations of precursors [e.g., *Guenther et al*., 2000; *Singh et al*., 2000; *Heikes et al*., 2002; *Jacob et al*., 2002; *Millet et al*., 2008; *Fischer et al*., 2012]. From eddy covariance (EC) measurements of air-sea flux, *Yang et al*. [2013b] showed that methanol is consistently deposited from the atmosphere to the surface ocean of the Atlantic. Based on in situ seawater and/or air concentrations, *Williams et al*. [2004] and *Carpenter et al*. [2004] predicted the ocean to be a net sink for atmospheric methanol, while *Beale et al*. [2013] suggested the ocean could be a net source as well as sink. Questions remain with regard to the spatial and temporal variability in air-sea methanol flux as well as the seawater methanol saturation. *Marandino et al*. [2005] and *Yang et al*. [2014] measured the air-sea acetone flux by EC and found the higher-latitude oceans to be net sinks of atmospheric acetone.

In the absence of direct measurements, the net air-sea gas flux is typically predicted from concentration gradients in either the airside or waterside using the two-layer model [*Liss and Slater*, 1974]:

$$Flux \approx K_a(C_w/H - C_a) \approx K_w(C_w - HC_a). \quad (1)$$

Here a positive flux indicates sea-to-air emission. C_w and C_a are the gas concentrations in bulk water and air. H is the dimensionless Henry's solubility (liquid to gas). C_w/H denotes an interfacial air concentration that would be in equilibrium with the underlying water, while HC_a represents an interfacial water concentration that would be in equilibrium with the overlaying air. The total gas transfer velocity from the perspective of airside concentration gradient (K_a) and waterside concentration gradient (K_w) are related by $K_a = HK_w$. We note that the assumption of flux continuity across the interface is valid only when production and consumption near the interface are insignificant.

K_a and K_w are composed of the individual transfer velocities in the air phase and water phase (k_a and k_w, respectively), with the relative importance of the two varying with gas solubility:

$$K_a = 1/(1/k_a + 1/(Hk_w)), \quad (2a)$$

$$K_w = 1/(1/k_w + \mathrm{H}/k_a). \quad (2b)$$

The air-sea transfer of sparingly soluble gases, such as carbon dioxide (CO_2) and dimethylsulfide (DMS), is controlled on the waterside (i.e., $K_w \approx k_w$). In contrast, the exchange of highly soluble gases like methanol is limited by airside resistance (i.e., $K_a \approx k_a$), with water vapor and sensible heat approaching pure airside control. Acetone represents an intermediate case between these two limiting regimes, as its transfer is influenced by both airside and waterside resistance. *McGillis et al.* [2000] defined the atmospheric gradient fraction γ_a as the fractional contribution to the total air-sea concentration gradient that is on the airside:

$$\gamma_a = 1/(1 + k_a/(Hk_w)). \quad (3)$$

At 20°C and in moderate winds, the COARE (Coupled Ocean-Atmosphere Response Experiment) model [*Fairall et al.*, 2011] predicts γ_a of approximately 0.006, 0.05, 0.7, and 1.0 for CO_2, DMS, acetone, and methanol, respectively.

Due to interests in the air-sea exchange of CO_2 and to a lesser extent DMS, quantifying k_w has been the focus for numerous studies in recent decades. However, uncertainties in the seldom-measured k_a may be as large as in k_w due to a paucity of direct observations and experimental verifications over the ocean [*Johnson*, 2010; *Johnson et al.*, 2011]. Values of k_a inferred from water vapor/sensible heat transfer from the laboratory [e.g., *Liss*, 1973; *Mackay and Yeun*, 1983] are about twice as high as those observed over the ocean. Analogously, laboratory measurements of k_a for trace gases may not be applicable to the open ocean [*Johnson*, 2010]. In addition to OVOCs, the air-sea exchange of many pollutants (e.g., sulfur dioxide, nitrogen oxides) and toxins (e.g., polychlorobiphenyls or PCBs) are also subject to significant airside resistance due to their high solubility or surface reactivity [*Duce et al.*, 1991].

Several models have tried to predict the air-sea exchange of gases of different solubility [e.g., *Fairall et al.*, 2011; *Pozzer et al.*, 2006; *Johnson*, 2010]. *Fairall et al.* [2007] incorporated waterside reactivity to estimate the atmospheric deposition of ozone. Recently, *He and Fu* [2013] proposed a "three-layer" model that explicitly considers a surface microlayer with photochemical and biological processes to explain the discrepancy between directly measured and predicted fluxes of acetone observed by *Marandino et al.* [2005]. Given these theoretical advances, it is clear that more direct observations of highly soluble/surface reactive gases over the ocean are necessary to validate models and improve our overall understanding in air-sea gas exchange. By simultaneously measuring the air-sea transfer of methanol and acetone with EC during the High Wind Gas Exchange Study (HiWinGS), we directly compute K_a from equation (1) and further constrain k_a and k_w.

2. Experiment

The HiWinGS cruise on board the RV *Knorr* started from Nuuk, Greenland on 9 October and finished in Woods Hole, USA on 14 November 2013. Fluxes of a number of gases were measured with the EC technique, including methanol and acetone (this paper), DMS (University of Hawaii), CO_2 (University of Hawaii and National Oceanographic and Atmospheric Administration), and hydrocarbons (University of California, San Diego). The ship was south of Greenland in the Labrador Sea for the first ~20 days of the cruise (Figure 1a). Low sea surface temperature (SST) of ~8°C and salinity of ~34.5 indicate the intrusion of Arctic

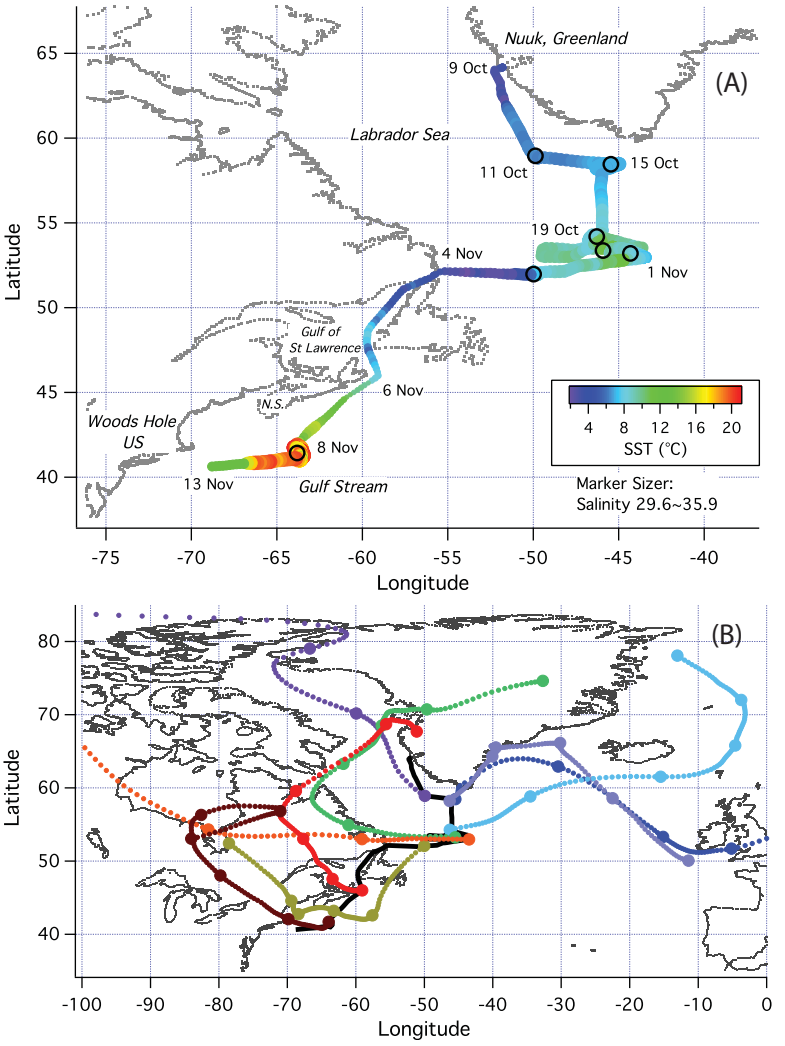

Figure 1. (a) Cruise track of HiWinGS, 2013, marked on selected dates. The color coding corresponds to sea surface temperature, while the marker size represents salinity. The black circles indicate the approximate station locations, where the ship held station with the bow-to-wind, usually for a few days at a time; (b) a zoomed out version of the cruise track showing 5 day air mass back trajectories initialized at a height of 50 m. Circles indicate daily intervals.

meltwater. After transiting through the Gulf of St Lawrence during 4–6 November, the ship was stationed south of Nova Scotia for the last week of the cruise, where SST and salinity were much higher at ~20°C and 36, respectively. As a part of the cruise strategy, the ship generally steamed on calm days to locations where storms were forecasted. Seven high wind speed stations were undertaken for deployments of wave instrumentations (University of Leeds, National Oceanography Center, Southampton, University of Southampton, National Oceanographic and Atmospheric Administration) concomitantly to EC flux measurements. When on station, the ship was positioned with the bow facing the wind. Hourly 10 m neutral wind speed (U_{10N}) ranged between 1 and 25 m s^{-1} and SST spanned from 2 to 21°C (Figure 2). Thus in addition to gas exchange, the HiWinGS cruise provided an excellent platform for validating of modeled air-sea momentum and heat fluxes.

2.1. Atmospheric Concentration Measurements

Methanol and acetone were measured using a high-sensitivity proton-transfer-reaction mass spectrometer (PTR-MS, Ionicon Analytik, Austria). The methods have been described in detail by *Yang et al.* [2013a, 2013b, 2014] and *Beale et al.* [2011]. We present a synopsis below and highlight the changes adopted for this cruise. The PTR-MS was located in a scientific lab van on the "02" deck of the ship, between the foredeck and bridge level. The Plymouth Marine Laboratory (PML) gas inlet, 3-D sonic anemometer, and motion

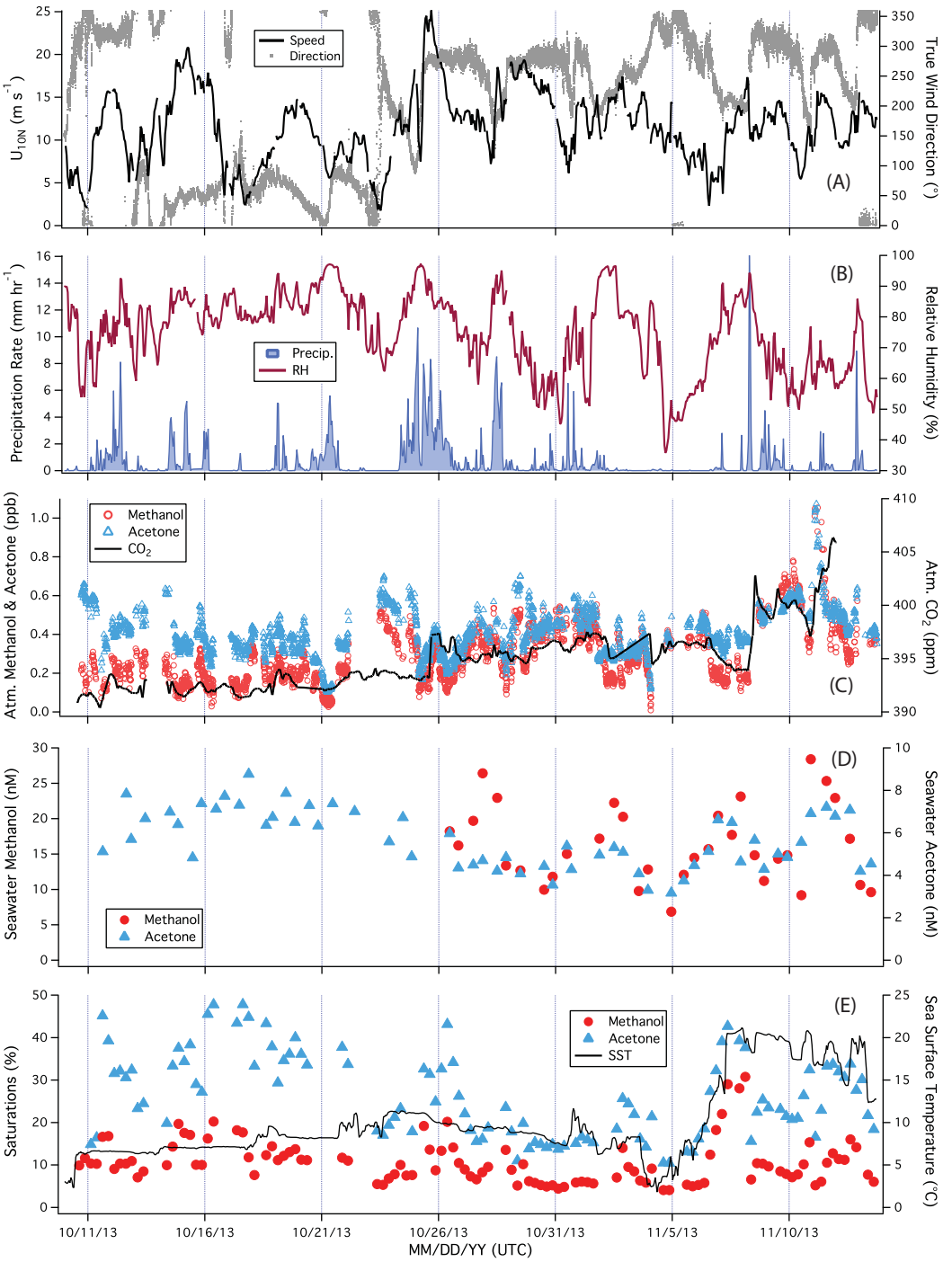

Figure 2. Time series of (a) 10 m neutral wind speed and wind direction; (b) rain rate and relative humidity; (c) atmospheric methanol, acetone, and CO_2 concentrations; (d) surface seawater methanol and acetone concentrations; (e) surface saturations of methanol, acetone, and sea surface temperature.

sensor were mounted on the foremast, ~20 m amsl and ~17 m from the bow of the ship. The opening of the gas inlet consisted of a downward facing Teflon (PTFE) elbow (3/8″ OD), which led to the lab van via ~15 m of 3/8″ OD Teflon (PFA) tubing. With a fully turbulent airflow (~30 L min^{-1}), the transit time in the manifold was ~1 s. The PTR-MS subsampled from the manifold at ~200 mL min^{-1}. Deuterated methanol (d3) and acetone (d6) gas standards in nitrogen (2.0 ± 0.1 ppm) were continuously injected into the manifold at a regulated flow of 30 sccm through a "tee" at ~20 cm behind the tip of the inlet. The isotopic

standard addition at the inlet tip not only provided continuous calibration, but should also account for any adsorptive loss of OVOCs in the manifold. As with *Yang et al*. [2013a, 2014], concentrations of methanol and acetone were computed from the ratios of the ambient and deuterated signals. The backgrounds in atmospheric concentrations were determined by directing ambient air through a platinum catalytic converter (350°C).

For air sampling, the PTR-MS cycled through m/z 21 ($H_3{}^{18}O^+$, dwell time of 20 ms), 32 (O_2^+, 20 ms), 33 ($CH_3OH{\bullet}H^+$, 200 ms), 36 ($CD_3OH{\bullet}H^+$, 50 ms), 59 ($CH_3COCH_3{\bullet}H^+$, 100 ms), and 65 ($CD_3COCD_3{\bullet}H^+$50 ms) in multiple ion detection mode, resulting in a total sampling frequency of ~2.2 Hz. The different dwell times at different masses were chosen to minimize instrument noise on the ambient methanol/acetone signals and maximize sampling frequency. We also monitored the levels of water dimers ($H_2O{\bullet}H_3O^+$) and isotopomers of standards from daily mass scans. The drift tube pressure of the PTR-MS (typically ~2.75 mbar) was set to maintain high sensitivity and also keep $H_2O{\bullet}H_3O^+$ less than 5% of the source ion signal. The PTR-MS source voltages influence the sensitivity of the instrument as well as the O_2^+ level. In a previous deployment [*Yang et al*., 2013b, 2014], the source ion count was $\sim 2.5 \times 10^7$ cps, while the sensitivities at m/z 33 and 59 were ~200 and 300 cps ppb^{-1}, respectively. O_2^+ was ~1% of the source ion signal, which resulted in a relatively low $^{16}O^{17}O^+$ count that was about half of the m/z 33 background. During HiWinGS, a different source voltage tuning was utilized to enhance instrument sensitivity. The source ion count increased from 2×10^7 cps at the beginning of the cruise to 4×10^7 cps toward the end, resulting in maximum sensitivities of ~300 and 400 cps ppb^{-1} at m/z 33 and 59, respectively. O_2^+, however, was ~2% of the source ion signal. The correspondingly higher $^{16}O^{17}O^+$ counts increased the background as well as noise level at m/z 33 during HiWinGS.

2.2. Seawater Concentration Measurements

Twice daily, seawater concentrations of methanol and acetone were measured with the PTR-MS coupled to a 3 m long silicon membrane heated to 50°C (described in detail by *Beale et al*. [2011]). The PTR-MS source/drift tube/detector voltage settings were identical for water and air sampling. By calibrating the system with freshly prepared aqueous standards, complete equilibration of the gas in the membrane was not required (and may not be achieved). However, due to the cold waters encountered during HiWinGS, the water temperature at the exit of the membrane did not always reach 50°C. Thus, variability in water temperature likely introduced some uncertainties in measured seawater concentrations. The seawater backgrounds were taken to be the signals when measuring the carrier gas flow (high-purity nitrogen passing through the same catalytic converter as used in air sampling). The water and air backgrounds were comparable (in the case of methanol, after accounting for the different $^{16}O^{17}O^+$ levels in air and in nitrogen).

Water samples were mostly taken from the CTD casts near the surface (2 or 5 m) and well below the pycnocline (500 m) in the morning and early evening each day. On the day of the largest storm of the cruise (25 October) and during transit, water samples from the ship's underway system were used. Repeated intercomparisons of surface CTD and underway samples while the ship was on station yielded comparable methanol concentrations. For acetone, the underway concentrations were consistently ~0.5 n*M* higher than the surface CTD values, presumably due to a slight contamination in the pumped supply. We corrected underway acetone concentrations by this offset. Seawater methanol concentration could not be quantified during the first half of the cruise due to a membrane fault. We therefore apply the mean seawater methanol concentration from the second half of the cruise to the first half in the calculations of saturation, expected flux, and K_a. As shown in section 3.4, computed K_a for methanol is not very sensitive to the seawater concentration because of the low saturation during HiWinGS.

2.3. Flux Computations

Air concentrations, winds, motion, and flow rates were all logged on the same computer, which was synchronized to the GPS clock daily. Measured winds were corrected for ship's motion following *Edson et al*. [1998] to yield true winds (u, v, w). We further decorrelate u, v, w with ship velocities and accelerations in their respective axis to remove residual motion cross correlation [*Edson et al*., 2011]. The corrected winds were used to compute the fluxes of OVOC ($\overline{w'OVOC'}$), sensible heat ($Q_H = \overline{w'T'_a}$), and momentum ($\tau = \overline{\rho w'u'}$) in hourly intervals. Here T_a is the temperature from the sonic anemometer corrected for humidity and ρ indicates air density.

Precipitation in the forms of squall, drizzle, and sleet were common during HiWinGS. Precipitation rate (10 min average) exceeded 5, 1, and 0.1 mm h^{-1} about 4, 16, and 32% of the time, with peak values over

50 mm h^{-1}. Averaged to hourly intervals, these thresholds were exceeded 4, 19, 41% of the time, respectively. The combination of precipitation and high winds contributed significant noise to the sonic anemometer measurements. We screened for this artifact by examining the variance and cospectra of *u*, *v*, *w* for substantially higher noise at frequencies >0.1 Hz. Other hourly criteria for valid momentum and heat fluxes include a relative wind direction within 90° from the bow and fairly constant ship heading (e.g., $\sigma < 40°$) as well as ship speed (e.g., $\sigma < 0.5$ m s^{-1}). Together these filters remove ~26% of the turbulent wind data (623 h remaining).

Because the gas intake was located ~17 m from the bow of the ship, contamination in air measurements from the ship's exhaust was sometimes apparent when the winds came from the side. Thus, we apply a more stringent set of hourly criteria for OVOC measurements: relative wind direction within 60° from the bow, σ in ship heading <10°, and range in ship heading <60°. Condensation and evaporation in the gas inlet, while not visually observed on this cruise, could affect high-frequency fluctuations in the atmospheric OVOC signals. We therefore discard OVOC fluxes when the relative humidity exceeded 85%. Lastly, large variations in atmospheric concentrations compromise the stationarity assumption of EC. Hourly periods are rejected when the range in methanol and acetone concentrations (minutely averaged) exceeded 0.4 and 0.3 ppb, respectively. Out of 594 h of OVOC fluxes recorded, ~300 h pass all of the aforementioned criteria.

Lag correlations of methanol and acetone with *w* generally yield comparable delays of ~5 s, consistent with the expected residence time in the inlet and PTR-MS. On several occasions during the cruise, we turned off the flow of the deuterated standard that was continuously injected into the gas inlet from the tip. Declines in the standard signals provided additional estimates for the time delay (also ~5 s) and high-frequency signal attenuation from the inlet. Atmospheric methanol concentration demonstrated a cross correlation with the ship's acceleration due to motion-induced variability in the $^{16}O^{17}O^{+}$ signal [*Yang et al*., 2013b, 2014]. Linearly decorrelating methanol with O_2^+ proves to be similarly effective as decorrelating with ship's motion; the former method is adopted for this cruise because of its simplicity. Lastly, we correct for high-frequency flux loss by using an empirical filter function approach [*Bariteau et al*., 2010; *Yang et al*., 2013a, 2014]. This correction is about15% and 23% at wind speeds of 10 and 20 m s^{-1}, respectively.

3. Results

3.1. Atmospheric Concentrations

Atmospheric methanol and acetone abundances were highly variable during HiWinGS, partly due to rapid shifts in wind directions and hence the sampling of different air masses during the passages of storms (Figure 2). Air mass back trajectories from the Hybrid Single-Particle Lagrangian Integrated Trajectory (HYSPLIT) model [*Draxler and Rolph*, 2013] for mainly the stations are shown in Figure 1b. Methanol and acetone concentrations averaged ~0.2 and 0.4 ppb during 10–22 October, when winds were mostly from the northern quadrant. The relatively low abundances are consistent with a paucity of surface sources for these compounds (e.g., terrestrial vegetation, anthropogenic emission, and biomass burning) in the Arctic and the higher latitudes of the North Atlantic. Over the next ~10 days, a shift in wind direction to westerly resulted in higher methanol concentrations of ~0.4 ppb, while acetone remained largely unchanged. Winds were predominantly from North America during the last week of the cruise. Mean concentrations of methanol and acetone increased to ~0.6 ppb, peaking over 1 ppb. As shown in Figure 2, atmospheric CO_2 also increased steadily as the ship transited from the Labrador Sea to the south of Nova Scotia.

A positive correlation is apparent between atmospheric methanol and acetone (Figure 3), similar to previous observations in terrestrial [e.g., *Schade and Goldstein*, 2006] and oceanic [e.g., *Yang et al*., 2014] environments. Both concentrations often decreased in the presence of rain and high humidity by similar proportions. Since acetone is about an order of magnitude less soluble than methanol, assuming near equilibrium between the gas phase and droplet phase, reduction in both compounds should not be due entirely to local scavenging by falling droplets (see section 4.3 for impact of wet deposition). The passage of different air masses likely also affected the atmospheric OVOC concentrations during storms [*Schade and Goldstein*, 2006]. The higher atmospheric OVOC and CO_2 levels further south highlight the importance of continental emissions. Furthermore, the methanol:acetone ratio tended to increase with the atmospheric abundance of CO_2. Compared to acetone, the more pronounced latitudinal gradient for methanol and the

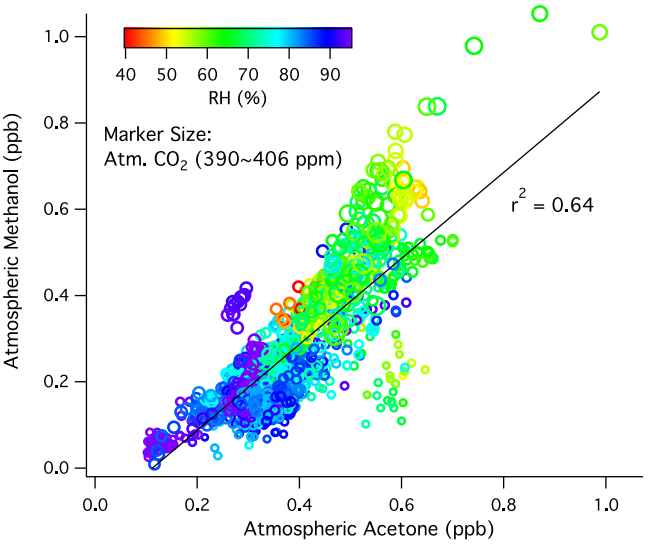

Figure 3. Atmospheric methanol and acetone abundances demonstrate a positive correlation. Both concentrations tended to be reduced at high relative humidity. The methanol:acetone ratio often increased with the atmospheric abundance of CO_2.

relationship with CO_2 were probably due to its shorter atmospheric lifetime and/or relatively greater input from terrestrial sources.

3.2. Seawater Concentrations and Surface Saturations

To the best of our knowledge, seawater OVOC concentrations have not been measured previously in high-latitude waters influenced by ice melt. Near-surface C_w of methanol and acetone had mean ($\pm$1 standard deviation, σ) values of $\sim$16.3 ($\pm$5.5) and 5.7 ($\pm$1.3) n*M* during HiWinGS (Figure 2), well above the detection limits of $\sim$6 and 0.3 n*M*, respectively [*Yang et al*., 2014]. These concentrations are generally lower than previous measurements in temperate waters [e.g., *Williams et al*., 2004; *Kameyama et al*., 2010; *Beale et al*., 2013]. To match the timestamp of the fluxes, smoothing interpolations were applied to the twice-a-day seawater concentrations. As with a previous deployment in the Atlantic [*Yang et al*., 2013b, 2014], atmospheric and seawater concentrations of these compounds were not significantly correlated ($r^2 \sim 0.05$ for both compounds). Saturations of methanol and acetone ($100C_w/(HC_a)$) were typically in the range of 5–20% (mean of 11%) and 10–40% (mean of 24%), respectively. Some higher saturation values were observed near Greenland where the atmospheric concentrations were low, as well as near the Gulf Stream where the SST was elevated. Methanol and acetone concentrations from $\sim$500 m depth were on average $\sim$80% and 70% of the surface values, respectively.

3.3. Turbulent Fluxes

Version 3.5 of the COARE model [*Edson et al*., 2013] is used to compute U_{10N}, bulk heat, and momentum fluxes. Compared to COARE 3.0 [*Fairall et al*., 2003], version 3.5 is refined through a modification of the wind speed-dependent Charnock coefficient and should provide better agreement with oceanic momentum measurements, especially in high winds.

The horizontal wind velocity relative to the earth was corrected for surface current to yield the wind speed over the ocean. The surface current velocity was estimated from Acoustic Doppler Current Profiler (ADCP) measurements in the upper $\sim$20 m of the ocean (mean speed of $\sim$0.3 m s^{-1}). The U. Hawaii sonic anemometer (Gill R2), located directly above the bow at 16.3 m amsl, should experience the least airflow distortion and observe the most representative mean ambient winds according to computational fluid dynamic modeling of the *Knorr* [*Moat and Yelland*, 1998]. When the relative wind direction was within 30° of the bow ($\sim$70% of the cruise time), U_{10N} from the U. Hawaii anemometer and the PML anemometer on the foremast demonstrate excellent agreement (slope of 0.99, $r^2 = 0.99$). With wind coming from the side of the ship ($\sim$10% of the cruise time), the PML anemometer overestimated wind speed by $\sim$5%. We thus plot our turbulent transfer estimates computed from the PML anemometer against the mean horizontal wind speed and modeled bulk estimates derived from the U. Hawaii anemometer.

Measured friction velocity ($u_* = (\overline{-w'u'})^{1/2}$) is largely consistent with prediction from the COARE 3.5 model (Figures 4 and 5a). Figure 5 shows u^* and the dimensionless 10 m neutral drag coefficient ($C_{D10N} = (u_*/U_{10N})^2$) as a function of U_{10N}. In high winds, model results from version 3.5 match our measurements more closely than version 3.0. At U_{10N} over 20 m s^{-1}, measured u^* and C_{D10N} still increase and show no sign of attenuation. C_{D10N} is more scattered at low-to-moderate wind speeds (when the ship was often under way) than at high wind speeds (when the ship was on station). This was in part due to an increase in the uncertainty associated with the motion correction when the ship was under way compared to when

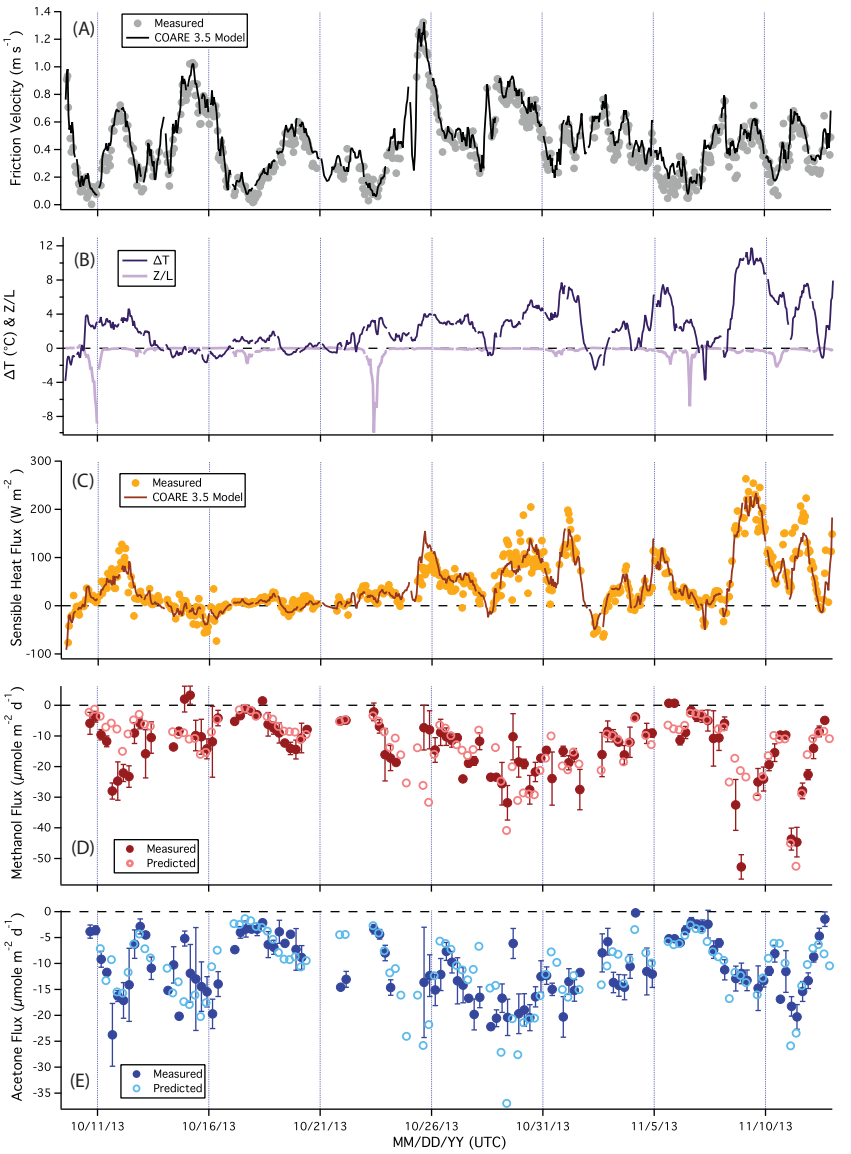

Figure 4. Time series of (a) friction velocity; (b) sea-air temperature difference and z/L; (c) sensible heat flux; (d) measured (6 h running average, with error bars corresponding to standard errors) and predicted (two-layer model) methanol flux; (e) measured (6 h running average, with error bars corresponding to standard errors) and predicted (two-layer model) acetone flux.

the ship was on station. When winds came from the side of the ship, the wind speed dependence in C_{D10N} appears to be reduced, possibly due to a minor distortion in airflow. We note that the derivation of C_{D10N}, scaled to $1/U_{10N}^2$, is more sensitive of flow distortion than the estimations of turbulent fluxes themselves. A dependence on wind direction is not observed in sensible heat and OVOC fluxes, suggesting that the impact of flow distortion on scalar transfer is minimal. Moreover, minor artifacts from flow distortion should presumably cancel when comparing transfer velocities of different scalars computed from the same wind data. Cospectra of momentum and sensible heat averaged to wind speed bins and a comparison of wind speed between the U. Hawaii and PML sonic anemometers can be found in Supporting Information.

The sea-air temperature difference ($\Delta T = SST$—potential air temperature) was mostly within a few °C in the Labrador Sea. On several occasions when the overlying air was warmer than the sea surface (e.g., 15, 19, 28 October; 2 November), the atmosphere remained near neutral as a result of strong winds. The dimensionless Monin-Obukhov stability parameter (z/L) from COARE 3.5 was above 0 and 0.05 for ~20% and ~2% of the cruise duration, respectively. Near the Gulf Stream, the surface water was warmer than the overlying air by up to ~10°C, resulting in large sensible heat fluxes (Q_H). To reduce noise in the computed sensible heat

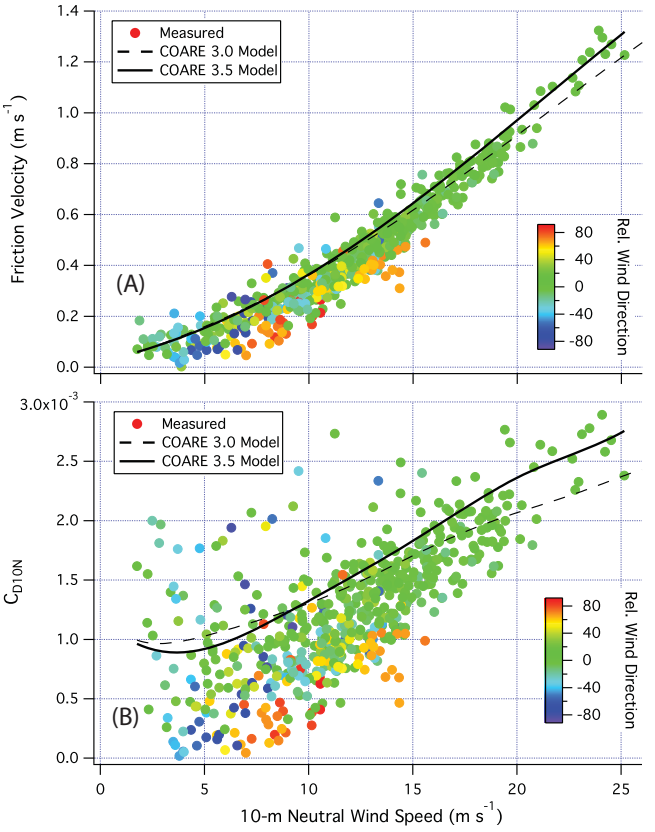

Figure 5. Hourly measured friction velocity and 10 m neutral drag coefficient versus 10 m neutral wind speed (hourly), color coded by relative wind direction (0 indicates wind from bow to stern). Parameterizations from versions 3.0 and 3.5 of the COARE model are also shown.

transfer velocity ($K_{Heat} = Q_H/\Delta T$) and dimensionless coefficient ($C_{H10N} = K_{Heat}/U_{10N}$), only hours when the magnitude of the air-sea temperature difference exceeded 1.5°C are considered further.

We adjust the transfer velocities of sensible heat and OVOCs to neutral atmospheric stability following similarity theory [*Fairall et al.*, 1996]. This assumes that sensible heat and OVOCs can be described by the same stability function as water vapor from COARE. Measured Q_H and the resultant K_{Heat} and C_{H10N} match well with the COARE 3.5 model predictions up to U_{10N} of 15 m s^{-1} (Figure 6). Between U_{10N} of 15 to 20 m s^{-1}, measured K_{Heat} and C_{H10N} are slightly higher than the COARE estimates, similar to findings from *Bell et al.* [2013]. We note that the upward adjustment of C_{D10N} in COARE 3.5 at high wind speeds has not been carried through to the model estimation of heat transfer. At the peak of the largest storm on 25 October, measured heat transfer was lower than predicted at U_{10N} over 20 m s^{-1}. During this period, the fairly low ΔT (2.5–3.8°C) limited the magnitude of sensible heat flux. Heavy precipitation (3–8 mm h^{-1}), high humidity (~90%), and likely large atmospheric loading of sea spray aerosols increased the flux uncertainties and could have caused a bias in the Q_H measurements. In particular, evaporation of spray droplets, which are concentrated in the wave boundary layer (the lowest few m above the ocean), cools the near-surface air and is expected to suppress the upward sensible heat flux [*Andreas et al.*, 1995].

3.4. Methanol and Acetone Transport

Time series (6 h running averages) of methanol and acetone fluxes are shown in Figure 4. Over the entire cruise, the average (±1 σ) methanol and acetone fluxes were −15 (±9) and −11 (±5) μmol m^{-2} d^{-1}, respectively. Greater fluxes were observed during periods of strong winds and high atmospheric concentrations. For example, methanol flux was elevated south of Nova Scotia due to the continental outflow. For acetone, the slightly higher atmospheric concentration there was partly compensated by the warmer waters (hence reduced solubility) near the Gulf Stream, resulting in fairly similar fluxes throughout the cruise.

For comparisons to the EC fluxes, methanol and acetone fluxes are predicted from equation (1) using in situ air/water concentrations, k_a and k_w from the COARE gas transfer model [*Fairall et al.*, 2000, 2011], and solubility from *Snider and Dawson* [1985] and *Zhou and Mopper* [1990]. The airside and waterside Schmidt numbers (Sc_a and Sc_w) are taken from *Johnson* [2010]. In the estimation of k_w, the COARE model empirical constant A for direct waterside transfer [*Hare et al.*, 2004] is set to 1.3 in agreement with transfer velocity measurements of DMS [*Blomquist et al.*, 2006; *Yang et al.*, 2011]. Due to the relatively high solubility of OVOCs, bubble-mediated exchange for these gases is thought to be negligible [*Woolf*, 1997] and thus neglected here for simplicity (empirical constant $B = 0$). As shown in Figure 4, measured and predicted

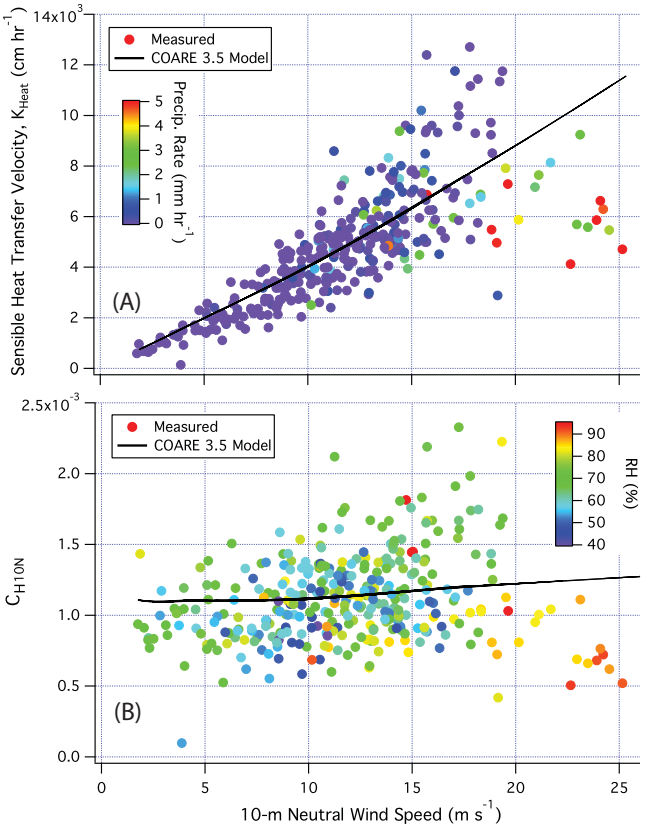

Figure 6. Hourly measured neutral sensible heat transfer velocity ((a) color coded by precipitation rate) and dimensionless transfer coefficient ((b) color coded by relative humidity) versus 10 m neutral wind speed.

fluxes of methanol and acetone demonstrate reasonable agreement, with relative root mean square error of 17 and 16%, respectively.

Measured total transfer velocities of methanol and acetone (K_a = Flux/($C_w/H - C_a$)) are plotted against U_{10N} in Figures 7 and 8. K_a is computed both hourly and from 6 h running averages of fluxes as well as air/water concentrations. To reduce random noise in the derived K_a, we only consider hours when the atmospheric concentration exceeded 0.2 ppb. A Schmidt number correction is not applied here since Sc_a (and hence k_a) is essentially constant with temperature. For both gases, measured K_a is similar to the COARE prediction up to U_{10N} of ~20 m s^{-1} but with considerable scatter. We briefly examine random uncertainties in the predicted flux and computed K_a due to the sparse (twice daily) water sampling. Because of the generally low surface saturations for methanol and acetone, their respective air-sea concentration gradients in equation (1) were dominated by C_a, while the influences of C_w were relatively small. For example, increasing/decreasing the seawater methanol concentration by 33% (1 σ) increases/decreases the computed K_a by only 5% and 4%, respectively. Increasing/decreasing the seawater acetone concentration by 24% (1 σ) increases/decreases the computed K_a by 9% and 7%, respectively. Further, the ship was on station for ~60% of the time during this cruise, which helped to minimize the impact of horizontal heterogeneity. C_w was also not statistically different between the morning and the late evening casts for both compounds, suggesting limited diel variation in these waters. Overall, fluctuations in C_w not captured by our sampling design mostly likely contributed to only minor (<10%) scatter in the predicted flux and computed K_a.

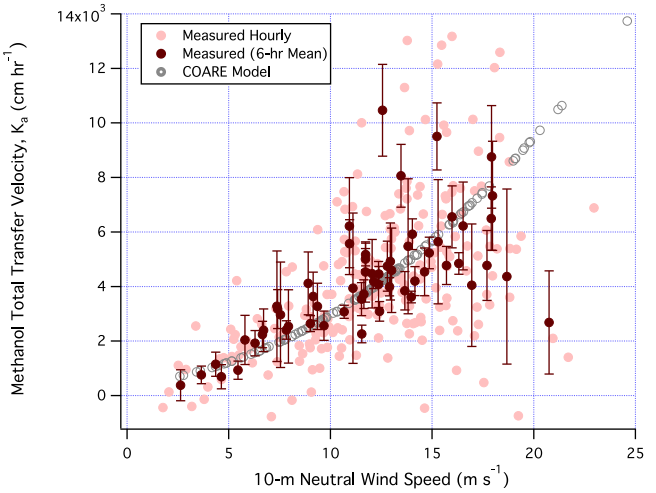

Figure 7. Measured neutral methanol transfer velocity versus 10 m neutral wind speed (hourly and 6 h running average). Error bars on the running average represent standard errors.

Qualitatively similar to K_{Heat}, K_a of OVOCs appears to be suppressed at the highest wind speeds, especially for methanol. The atmospheric concentrations of these compounds were relatively low during the 25 October storm, which, in addition to the severe environmental conditions, resulted in noisy flux measurements. The role of sea spray on the air-sea

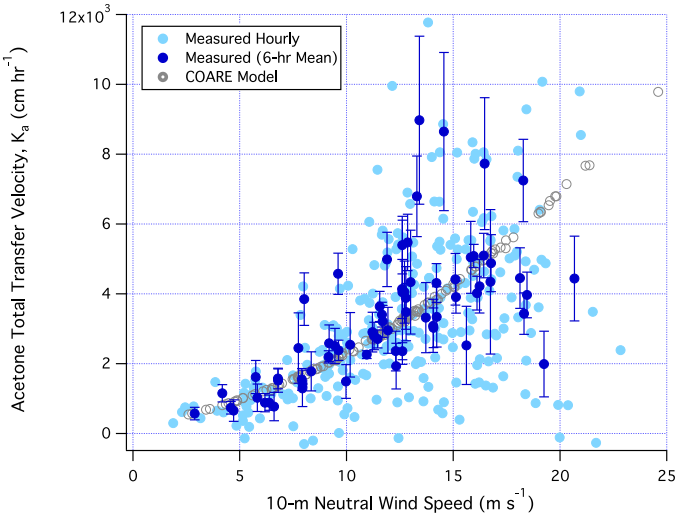

Figure 8. Measured neutral acetone transfer velocity versus 10 m neutral wind speed (hourly and 6 h running average). Error bars on the running average represent standard errors.

exchange of airside controlled compounds remains highly uncertain. Complete evaporation of sea spray droplets should release any dissolved methanol and acetone into the lowest few meters of the atmosphere, thereby possibly reducing the air-to-sea fluxes of these compounds (I. Brooks, personal communication, 2014). Interestingly, from a cruise in the North Atlantic, *Bell et al*. [2013] observed reduced transfer velocity of DMS at wind speeds of 15–20 m s^{-1} and in the presence of large waves. The air-sea transfer of DMS (mainly waterside limited) and OVOCs (mainly airside limited) are governed by different physical processes. Swell may suppress microscale breaking [*Banner et al*., 1989], which is considered the main driver for waterside interfacial gas transfer; this process probably does not significantly affect airside transfer. Flow separation, or shielding the troughs of swell from wind shear [*Veron et al*., 2007], could possibly reduce the airside transfer as well as waterside transfer. These possibilities will be tested once the evaluation of the wave data collected during the cruise has been completed. In the following analysis, we neglect hourly OVOC transfer data when U_{10N} exceeded 20 m s^{-1}.

4. Discussion

4.1. Quantification of k_a and k_w

Wind stress at the surface drives turbulent transport and disrupts the molecular sublayers on both sides of the interface, resulting in increased k_a as well as k_w. The air phase transfer velocity is inversely related to the sum of turbulent (aerodynamic) resistance (R_t) and molecular diffusional resistance (R_m): $k_a = 1/(R_t + R_m)$. Parameterizations of k_a differ in their wind speed dependence as well as in the normalization between different compounds (see summary by *Johnson* [2010]). Based on wind tunnel measurements, *Liss* [1973] found a linear relationship between the rate of H_2O transfer and wind speed; k_a for a heavier gas is slower than that of H_2O by a factor proportional to the square root of molecular weight [*Liss and Slater*, 1974]. This molecular weight (MW) scaling was later adopted by *McGillis et al*. [2000]. *Mackay and Yeun* [1983] measured the volatilization rates of a number of trace gases from a wind-wave tank; they derived a linear dependence for k_a on u^* and a $-2/3$ power for Sc_a. Based on the works of *Hicks et al*. [1986], *Duce et al*. [1991] applied a $Sc_a^{-2/3}$ (or $MW^{-1/3}$) normalization to only the airside molecular transfer ($1/R_m$); a linear dependence of turbulent transfer ($1/R_t$) on wind speed is specified in their formulation by using a fixed C_D. A similar resistance-based approach is adopted by the COARE model, which incorporates a wind speed-dependent C_D for $1/R_t$ and a $Sc_a^{-1/2}$ scaling for $1/R_m$.

Measured K_a (total transfer velocity) of acetone linearly correlates with that of methanol with a slope of 0.72($\pm$0.03) and r^2 of 0.82 during HiWinGS (Figure 9). Compared to methanol, K_a for acetone is lower because (1) acetone is less soluble and so faces greater waterside control and (2) it diffuses more slowly in air by virtue of its larger molecular weight. In the cold waters of HiWinGS, the atmospheric gradient fraction γ_a computed from COARE was 0.98 and 0.79 for methanol and acetone, respectively (i.e., $K_a \approx k_a$ for methanol). Due to the difference in their solubility, the ratio in total transfer velocity (K_a) between acetone and methanol would be 0.81 (=0.79/0.98) if the air phase transfer velocity (k_a) were equal for these two compounds.

Acetone has a lower molecular diffusivity in air, and so a higher Sc_a (1.55) than methanol (1.09). At moderate wind speeds, estimates for the expected ratio in k_a between acetone and methanol are ~0.74 [*Liss*, 1973;

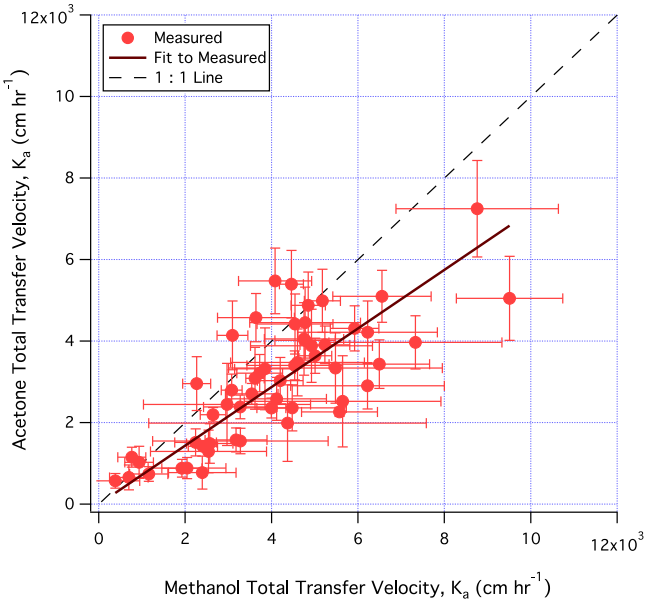

Figure 9. Measured neutral transfer velocities of acetone versus methanol (6 h average, error bars correspond to standard error).

Liss and Slater, 1974], 0.80 [*Mackay and Yeun*, 1983], 0.97 [*Duce et al.*, 1991], and 0.92 (COARE). Multiplying these expected ratios of k_a by 0.81 (i.e., to account for the solubility difference) leads to predicted ratios in the total transfer velocity (K_a) between acetone and methanol of 0.60 and 0.65, 0.79, and 0.75. The measured ratio in K_a, again, is 0.72(±0.03). Thus, normalizing k_a (instead of $1/R_m$) by a MW or Sc_a dependence likely leads to too large of a divergence between these two compounds. Scaling from the COARE model, which treats aerodynamic and molecular diffusion terms separately, seems to be the most consistent with our measurements.

The transfer velocity of sensible heat correlates linearly with that of methanol with a slope of 1.12 (±0.05) and r^2 of 0.95 (Figure 10). The COARE model predicts a ratio between heat and methanol of 1.11. Methanol transfer is slower mostly because of its lower airside diffusivity, and hence higher Sc_a (1.09) compared to heat (0.64). Errors in the measurements, uncertainty in the magnitude of $1/R_m$, and the limited dynamic range in Sc_a between these scalars preclude an exact determination of the exponent in the airside molecular diffusion term (i.e., $Sc_a^{-2/3}$ or $Sc_a^{-1/2}$).

Simultaneous K_a measurements of gases with different solubility allows us to constrain the magnitude of not only k_a, but also k_w:

$$k_w = 1/(H(1/K_a - 1/k_a)). \quad (4)$$

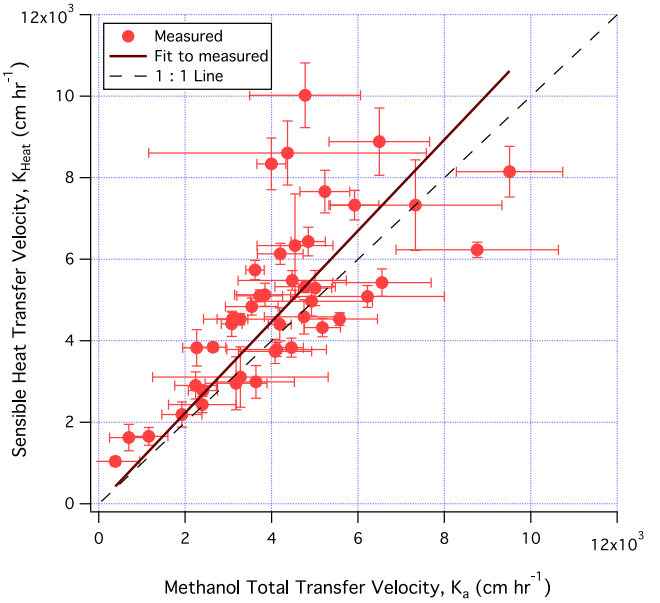

Figure 10. Measured neutral transfer velocities of sensible heat versus methanol (6 h average, error bars correspond to standard error).

The mean dimensionless solubility and waterside Schmidt number for acetone are 1400 and 2000 for HiWinGS, respectively. Crudely equating K_a of methanol to k_a of acetone and using the measured K_a for acetone, we compute a mean k_w of 7.8 (±3.1) cm h^{-1} for the entire cruise. The uncertainty here is propagated from 15% independent error for both measured K_a. Normalizing this k_w to a waterside Schmidt number of 660 following a $Sc_w^{-1/2}$ relationship yields a k_{w660} of 13.6 (±5.4) cm h^{-1} at a mean U_{10N} of 12 m s^{-1}. If we combine the measured K_a and modeled k_a of acetone from COARE, from equation (4) we arrive at 9.1 (±4.3) and 15.9 (±7.4) cm h^{-1} for k_w and k_{w660}, respectively. Resistance on the waterside becomes more important at

higher temperatures due to a decrease in gas solubility [*McGillis et al*., 2000]. Thus, the accuracy of this k_w estimation may be improved by measuring in warmer waters or by quantifying the transfer of another gas with greater waterside control.

It is instructive to compare these results to other estimates of the waterside transfer velocity at $Sc_w = 660$ and $U_{10N} = 12$ m s^{-1}. From an analysis of air-sea DMS exchange, *Yang et al*. [2011] estimated a total waterside transfer velocity of ~22 (±1) cm h^{-1} and a tangential (shear driven) transfer velocity of ~18 (±1) cm h^{-1}, with the difference between the two attributed to bubble-mediated effects. With model empirical constants of $A = 1.3$ and $B = 1$, COARE similarly predicts 22 cm h^{-1} for the total DMS transfer velocity and 19 cm h^{-1} for the tangential transfer velocity. From measurements of the sparingly soluble ^{3}He/SF_6 or CO_2, previous estimates of k_{w660} at $U_{10N} = 12$ m s^{-1} include 34 cm h^{-1} [*Nightingale et al*., 2000], 48 cm h^{-1} [*McGillis et al*., 2001], 37 cm h^{-1} [*Ho et al*., 2006], and 39 cm h^{-1} [*Sweeney et al*., 2007]. Our k_{w660} derived above is in reasonable agreement with the tangential transfer velocity from DMS, which is consistent with reduced bubble-mediated gas transfer for a soluble gas such as acetone. k_{w660} obtained from sparingly soluble gases is understandably larger due to the additional transfer induced by bubbles. This suggests that a $Sc_w^{-1/2}$ relationship does not adequately account for the variable importance of bubble-mediated transfer among different gases.

4.2. Comparison With Previous OVOC Flux Estimates

The magnitude and direction of methanol flux during HiWinGS are consistent with observations in the North Atlantic during the 2012 Atlantic Meridional Transect (AMT-22) cruise [*Yang et al*., 2013b]. For AMT-22, K_a computed from the EC flux sometimes exceeded the aerodynamic limit as well as the observed rate of sensible heat transfer when using the measured seawater concentration (mean of 29 n*M*, saturation of ~30%); a more physically reasonable K_a was obtained when adopting a reduced C_w (by >50%). Due to a combination of low seawater concentration and SST, the surface methanol saturation from HiWinGS was only ~1/3 of that during AMT-22; thus, in this case, K_a is not very sensitive to the value of C_w. During HiWinGS, the dimensionless methanol and acetone transfer coefficients (K_a/u^*) have mean values (±SE) of 0.031 (±0.002) and 0.023 (±0.001), respectively. Calculated as a purely depositional process (C_w set to 0), the dimensionless methanol and acetone "deposition coefficients" ($Flux/-C_a/u^*$) are 0.028 (±0.001) and 0.019 (±0.001). The mean methanol transfer coefficient during HiWinGS is, within measurement uncertainties, in agreement with the mean dimensionless methanol deposition coefficient of 0.031 (±0.001) observed on AMT-22.

Marandino et al. [2005] measured the air-sea acetone flux by EC and the seawater acetone concentration from the ship's underway intake on a transit cruise in the Pacific. At higher latitudes, their measured influx (deposition) by EC was consistent with prediction from the two-layer model based on air/sea concentrations. However, near the tropics they measured an influx by EC while the model predicted efflux (emission) due to the large underway seawater concentrations. This inconsistency between EC and predicted acetone fluxes was not observed during the AMT-22 cruise by *Yang et al*. [2014], who reported deposition at higher latitudes and emission in the subtropics. Similarly, acetone flux was always from the atmosphere to the ocean during HiWinGS, in accord with air/sea concentrations.

Interestingly, *Marandino et al*. [2005] reported a slope of -5.84×10^{-4} (dimensionless) between EC Flux/U_{10N} (pmol m^{-3}) and C_a (nmol m^{-3}). For the HiWinGS data set, we find a very similar slope through zero of -5.4×10^{-4} between these two variables (Figure 11). This negative relationship implies a weak dependence of the flux on C_w, which during HiWinGS is likely due to the low saturation of acetone. Together with results from *Yang et al*. [2014] and *Beale et al*. [2013], it appears that the net acetone flux is from air-to-sea in the higher latitudes of the North Atlantic and Pacific, confirming the global model predictions of *Fischer et al*. [2012].

4.3. Dry, Wet Deposition Fluxes and Residence Times

Atmospheric methanol and acetone generally decreased with increasing relative humidity and precipitation rate during HiWinGS (Figure 3). This should not be a measurement artifact (e.g., adsorption onto the inlet wall) because the isotopic standards were introduced close to the inlet tip and should be subject to comparable humidity effects. It is instructive to compare the dry (EC) and wet deposition fluxes of these compounds. Large dissolved concentrations of methanol (on the order of 1 μM) have been measured in rainwater samples from terrestrial sites [*Snider and Dawson*, 1985; *Felix et al*., 2014]. These values appear to be near thermodynamic equilibrium with the gas phase, as might be expected for an upper limit estimate

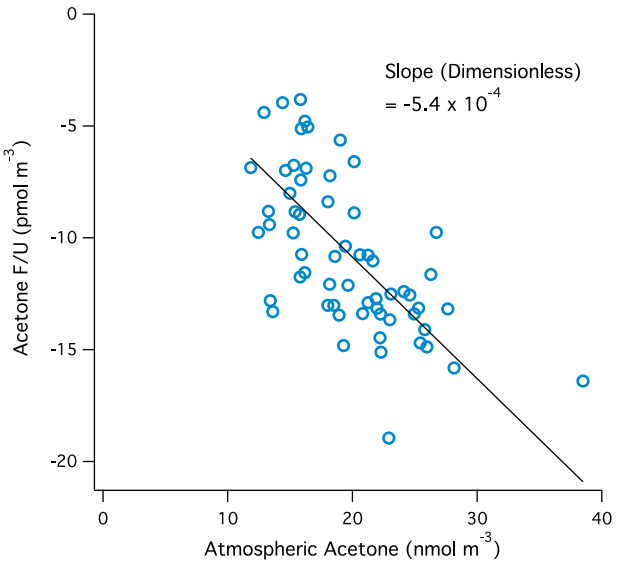

Figure 11. Relationship between flux divided by wind speed and the atmospheric concentration of acetone (to be compared to *Marandino et al*. [2005, Figure 3]). Note the different units between the abscissa and ordinate.

in the absence of any production and consumption in rainwater. Assuming equilibrium at ambient air temperature, we estimate the wet deposition flux of OVOCs as the product of the hourly averaged precipitation rate and HC_a. The mean wet deposition of methanol of ~ -3 μmol m^{-2} d^{-1} is about 20% of the mean dry deposition flux. During heavy precipitation events, the magnitude of wet deposition for methanol, on the order of -50 μmol m^{-2} d^{-1}, exceeds dry deposition. For acetone, because of its lower solubility, the mean and maximum wet deposition fluxes are lower at ~ -0.5 and -8 μmol m^{-2} d^{-1}; these are typically smaller in magnitude than the EC flux.

Calculated from the HiWinGS data set for a 1 km high marine atmospheric boundary layer with 0.4 ppb of methanol and 0.5 ppb of acetone, dry deposition removes these compounds on time scales of $\sim$1 and 2 days. These are significantly shorter than the most recent estimates of the global atmospheric lifetimes of methanol (4.7 days) [*Millet et al*., 2008] and acetone (14 days) [*Fischer et al*., 2012], values that include the free troposphere. Removal of these compounds due to air-sea exchange might be especially rapid in this study region due to the low saturations and elevated wind speeds. The mean atmospheric lifetime of methanol and acetone during HiWinGS due to wet deposition is longer at 6 and 43 days, respectively. Heavy precipitation events, however, can remove these compounds as quickly as $\sim$0.3 and 3 days.

Was atmospheric deposition sufficient to sustain the observed dissolved OVOC concentrations during HiWinGS? For a 50 m mixed layer with 16 n*M* of methanol and 6 n*M* of acetone, the respective replacement time by atmospheric deposition (sum of dry and wet fluxes) is 44 and 26 days. In comparison, the removal time due to microbial oxidation in the surface open ocean is on the order of 1–10 days for methanol [*Dixon et al*., 2011, 2013] and 5–55 days for acetone [*Dixon et al*., 2013]. Faster microbial acetone oxidations have been reported in winter (turnover time from $<$1 to 3 days) than in summer based on studies near the coast [*de Bruyn et al*., 2013; *Dixon et al*., 2014]. Thus, atmospheric input alone was probably not enough to account for the mixed layer OVOC stocks during HiWinGS. Rapid biological consumption and limited in situ production contributed to the relatively low dissolved OVOC concentrations, which, together with high solubility in cold waters, led to significant undersaturation and net air-to-sea transport of these compounds.

5. Conclusion

The air-sea fluxes and dissolved concentrations of methanol and acetone were measured concurrently during HiWinGS. The surface ocean, depleted in dissolved methanol and acetone relative to the atmosphere, consistently acted as a net sink for both of these compounds. Measured transfer velocities of the predominantly airside controlled methanol and acetone are similar to those predicted by the COARE model. This is reasonable, as the COARE model predicts momentum and heat transport fairly well, which are also airside controlled. Comparing the transfer of methanol, acetone, and sensible heat allows us to examine the Sc_a scaling in the air phase transfer velocity (k_a) and also constrain the magnitude of the water phase transfer velocity (k_w). Our estimated k_w supports the previously determined tangential (shear driven) waterside transfer velocity, and is lower than k_w derived from sparingly soluble gases, for which bubble-mediated transport has been predicted to be dominant at high wind speeds. Lastly, we estimated the wet deposition fluxes of these compounds assuming equilibrium between gas phase and droplet concentrations. Wet

deposition flux is similar in magnitude to or greater than the EC (dry deposition) flux during heavy precipitation events for methanol, but is less significant for acetone. Total atmospheric deposition removes methanol and acetone from the lower atmosphere with a short time scale of 1–2 days. However, atmospheric input was likely not enough to sustain the dissolved concentrations of these compounds in the oceanic mixed layer.

Acknowledgments

This work is supported by the U.S. National Science Foundation (grant OISE-1064405), the United Kingdom Natural Environment Research Council, and the PML Kingsland Fellowship. B.W.B. acknowledges support from NSF grant ATM10-36062. Data from this cruise will be uploaded on to the NOAA FTP server and made publicly available within 2 years from the completion of the cruise. We gratefully acknowledge the National Oceanic and Atmospheric Administration Air Resources Laboratory for the provision of the HYSPLIT transport and dispersion model and READY web site (http://ready.arl.noaa.gov). We would like to thank M. Kim and R. Pascal for instrumentation setup, L. Bariteau for the compilation the meteorological measurements, J. Hummon for the processing of ADCP data, R. Feely for underway CO_2 measurements, R. Beale and T. Bell for scientific input, and finally P. *Liss*, B. Huebert, and C. Fairall for continued guidance. Special thanks to the crew of the *Knorr* for their dedication during this stormy cruise.

References

Andreas, E. L., J. B. Edson, E. C. Monahan, M. P. Rouault, and S. D. Smith (1995), The spray contribution to net evaporation from the sea, *Boundary Layer Meteorol.*, *72*, 3–52.

Banner, M. L., I. S. F. Jones, and J. C. Trinder (1989), Wave number spectra of short gravity waves, *J. Fluid Mech.*, *198*, 321–344, doi:10.1017/S0022112089000157.

Bariteau, L., D. Helmig, C. Fairall, J. Hare, J. Hueber, and E. Lang (2010), Determination of oceanic ozone deposition by ship-borne eddy covariance flux measurements, *Atmos. Meas. Tech.*, *3*, 441–455, doi:10.5194/amt-3-441-2010.

Beale, R., J. Dixon, P. Liss, and P. Nightingale (2011), Quantification of oxygenated volatile organic compounds in seawater by membrane inlet-proton transfer reaction/mass spectrometry, *Anal. Chim. Acta*, *706*, 128–134.

Beale, R., J. Dixon, S. Arnold, P. Liss, and P. Nightingale (2013), Methanol, acetaldehyde and acetone in the surface waters of the Atlantic Ocean, *J. Geophys. Res. Oceans*, *118*, 5412–5425, doi:10.1002/jgrc.20322.

Bell, T. G., W. De Bruyn, S. Miller, B. Ward, K. Christensen, and E. Saltzman (2013), Air–sea dimethylsulfide (DMS) gas transfer in the North Atlantic: Evidence for limited interfacial gas exchange at high wind speed, *Atmos. Chem. Phys.*, *13*, 11,073–11,087, doi:10.5194/acp-13-11073-2013.

Blomquist, B., C. Fairall, B. Huebert, D. Kieber, and G. Westby (2006), DMS sea-air transfer velocity: Direct measurements by eddy covariance and parameterization based on the NOAA/COARE gas transfer model, *Geophys. Res. Lett.*, *33*, L07601, doi:10.1029/2006GL025735.

Carpenter, L. J., A. C. Lewis, L. R. Hopkins, K. A. Read, I. D. Longley, and M. W. Gallagher (2004), Uptake of methanol to the North Atlantic Ocean surface, *Global Biogeochem. Cycles*, *18*, GB4027, doi:10.1029/2004GB002294.

Carpenter, L. J., S. D. Archer, and R. Beale (2012), Ocean-atmosphere trace gas exchange, *Chem. Soc. Rev.*, *41*, 6473–6506.

de Bruyn, W. J., C. D. Clark, L. Pagel, and H. Singh (2013), Loss rates of acetone in filtered and unfiltered coastal seawater, *Mar. Chem.*, *150*, 39–44, doi:10.1016/j.marchem.2013.01.003.

Dixon, J., R. Beale, and P. Nightingale (2011), Rapid biological oxidation of methanol in the tropical Atlantic: Significance as a microbial carbon source, *Biogeosciences*, *8*, 2707–2716, doi:10.5194/bg-8-2707-2011.

Dixon, J. L., R. Beale, and P. Nightingale (2013), Production of methanol, acetaldehyde, and acetone in the Atlantic Ocean, *Geophys. Res. Lett.*, *40*, 4700–4705, doi:10.1002/grl.50922.

Dixon, J. L., R. Beale, S. Sargeant, G. Tarran, and P. Nightingale (2014), Microbial acetone oxidation in coastal seawater, *Frontiers Microbiol.*, *5*, 1–9, doi:10.3389/fmicb.2014.00243.

Draxler, R., and G. Rolph (2013), HYSPLIT model. NOAA Air Resources Laboratory, College Park, Md. [Available at http://ready.arl.noaa.gov/HYSPLIT.php, last accessed 16 Jul. 2014.]

Duce, R., et al. (1991), The atmospheric input of trace species to the World Ocean, *Global Biogeochem. Cycles*, *5*, 193–259.

Duncan, B., J. A. Logan, I. Bey, I. A. Megretskaia, R. M. Yantosca, P. C. Novelli, N. B. Jones, and C. P. Rinsland (2007), Global budget of CO, 1988–1997: Source estimates and validation with a global model, *J. Geophys. Res.*, *112*, D22301, doi:10.1029/2007JD008459.

Edson, J., A. Hinton, K. Prada, J. Hare, and C. Fairall (1998), Direct covariance flux estimates from mobile platforms at sea, *J. Atmos. Oceanic Technol.*, *15*, 547–562.

Edson, J. B., C. W. Fairall, L. Bariteau, C. J. Zappa, A. Cifuentes-Lorenzen, W. R. McGillis, S. Pezoa, J. E. Hare, and D. Helmig (2011), Direct covariance measurement of CO_2 gas transfer velocity during the 2008 Southern Ocean gas exchange experiment: Wind speed dependency, *J. Geophys. Res.*, *116*, C00F10, doi:10.1029/2011JC007022.

Edson, J. B., V. Jampana, R. A. Weller, S. P. Bigorre, A. J. Plueddemann, C. W. Fairall, S. D. Miller, L. Mahrt, D. Vickers, and H. Hersbach (2013), On the exchange of momentum over the open ocean, *J. Phys. Oceanogr.*, *43*, 1589–1610, doi:10.1175/JPO-D-12-0173.1.

Fairall, C. W., E. Bradley, R. Rogers, J. Edson, and G. Young (1996), Bulk parameterization of air-sea fluxes for tropical ocean-global atmosphere coupled-ocean atmosphere response experiment, *J. Geophys. Res.*, *101*, 3747–3764.

Fairall, C. W., J. E. Hare, J. E. Edson, and W. McGillis (2000), Parameterization and micrometeorological measurement of air-sea gas transfer, *Boundary Layer Meteorol.*, *96*, 63–105.

Fairall, C. W., E. Bradley, J. Hare, A. Grachev, and J. Edson (2003), Bulk parameterization of air-sea fluxes: Updates and verification for the COARE algorithm, *J. Clim.*, *16*, 571–591.

Fairall, C. W., J. E. Hare, D. Helmig, and L. Ganzveld (2007), Water-side turbulence enhancement of ozone deposition to the ocean, *Atmos. Chem. Phys.*, *7*, 443–451, doi:10.5194/acp-7-443-2007.

Fairall, C. W., M. Yang, L. Bariteau, J. Edson, D. Helmig, W. McGillis, S. Pezoa, J. Hare, B. Huebert, and B. Blomquist (2011), Implementation of the coupled ocean-atmosphere response experiment flux algorithm with CO_2, dimethyl sulfide, and O_3, *J. Geophys. Res.*, *116*, C00F09, doi:10.1029/2010JC006884.

Felix, J. D., S. B. Jones, G. B. Avery, J. D. Willey, R. N. Mead, and R. J. Kieber (2014), Temporal and spatial variations in rainwater methanol, *Atmos. Chem. Phys. Discuss.*, *14*, 1375–1398, doi:10.5194/acpd-14-1375-2014.

Fischer, E. V., D. J. Jacob, D. B. Millet, R. M. Yantosca, and J. Mao (2012), The role of the ocean in the global atmospheric budget of acetone, *Geophys. Res. Lett.*, *39*, L01807, doi:10.1029/2011GL050086.

Guenther, A., C. Geron, T. Pierce, B. Lamb, P. Harley, and R. Fall (2000), Natural emissions of non-methane volatile organic compounds; carbon monoxide, and oxides of nitrogen from North America, *Atmos. Environ.*, *34*, 2205–2230.

Hare, J. E., C. W. Fairall, W. R. McGillis, J. B. Edson, B. Ward, and R. Wanninkhof (2004), Evaluation of the National Oceanic and Atmospheric Administration/Coupled-Ocean Atmospheric Response Experiment (NOAA/COARE) air-sea gas transfer parameterization using GasEx data, *J. Geophys. Res.*, *109*, C08S11, doi:10.1029/2003JC001831.

He, C. L., and T. M. Fu (2013), Air-sea exchange of volatile organic compounds: A new model with microlayer effects, *Atmos. Oceanic Sci. Lett.*, *6*(2), 97–102.

Heald, C. L., et al. (2008), Total observed organic carbon (TOOC) in the atmosphere: A synthesis of North American observations, *Atmos. Chem. Phys.*, *8*, 2007–2025, doi:10.5194/acp-8-2007-2008.

Heikes, B. G., et al. (2002), Atmospheric methanol budget and ocean implication, *Global Biogeochem. Cycles*, *16*(4), 1133, doi:10.1029/2002GB001895.
Hicks, B. B., M. L. Wesely, S. E. Lindberg, and S. M. Bromberg (Eds.) (1986), Proceedings of the Dry Deposition Workshop of the National Acid Precipitation Assessment Program, NOAA!ATDD, Oak Ridge, Tenn.
Ho, D., C. S. Law, M. J. Smith, P. Schlosser, M. Harvey, and P. Hill (2006), Measurements of air-sea gas exchange at high wind speeds in the Southern Ocean: Implications for global parameterizations, *Geophys. Res. Lett.*, *33*, L16611, doi:10.1029/2006GL026817.
Jacob, D. J., B. D. Field, E. M. Jin, I. Bey, Q. Li, J. A. Logan, R. M. Yantosca, and H. B. Singh (2002), Atmospheric budget of acetone, *J. Geophys. Res.*, *107*(D10), 4100, doi:10.1029/2001JD000694.
Johnson, M. (2010), A numerical scheme to calculate temperature and salinity dependent air-water transfer velocities for any gas, *Ocean Sci.*, *6*, 913–932, doi:10.5194/osd-7-251-2010.
Johnson, M., C. Hughes, T. Bell, and P. Liss (2011), A Rumsfeldian analysis of uncertainty in air-sea gas exchange, in *Gas Transfer at Water Surfaces*, pp. 464–485, Kyoto Univ. Press, Kyoto, Japan.
Kameyama, S., H. Tanimoto, S. Inomata, U. Tsunogai, A. Ooki, S. Takeda, H. Obata, A. Tsuda, and M. Uematsu (2010), High-resolution measurement of multiple volatile organic compounds dissolved in seawater using equilibrator inlet–proton transfer reaction-mass spectrometry (EI–PTR-MS), *Mar. Chem.*, *122*, 59–73.
Liss, P. S. (1973), Processes of gas exchange across an air-water interface, *Deep Sea Res. Oceanogr. Abstr.*, *20*(3), 221–238, doi:10.1016/0011-7471(73)90013-2.
Liss, P. S., and P. G. Slater (1974), Flux of gases across the air-sea interface, *Nature*, *247*, 181–184, doi:10.1038/247181a0.
Mackay, D., and A. Yeun (1983), Mass transfer coefficient correlations for volatilization of organic solutes from water, *Environ. Sci. Technol.*, *17*, 211–217.
Marandino, C. A., W. J. De Bruyn, S. D. Miller, M. J. Prather, and E. J. Saltzman (2005), Oceanic uptake and the global atmospheric acetone budget, *Geophys. Res. Lett.*, *32*, L15806, doi:10.1029/2005GL023285.
McGillis, W. R., J. W. H. Dacey, N. M. Frew, E. J. Bock, and R. K. Nelson (2000), Water-air flux of dimethylsulfide, *J. Geophys. Res.*, *105*, 1187–1193.
McGillis, W. R., J. B. Edson, J. E. Hare, and C. W. Fairall (2001), Direct covariance air-sea CO_2 fluxes, *J. Geophys. Res.*, *106*, 16,729–16,745.
Millet, D. B., et al. (2006), Formaldehyde distribution over North America: Implications for satellite retrievals of formaldehyde columns and isoprene emission, *J. Geophys. Res.*, *111*, D24S02, doi:10.1029/2005JD006853.
Millet, D. B., et al. (2008), New constraints on terrestrial and oceanic sources of atmospheric methanol, *Atmos. Chem. Phys.*, *8*, 6887–6905, doi:10.5194/acp-8-6887-2008.
Moat, B. I., and M. J. Yelland (1998), Airflow distortion at instrument sites on the RV Knorr, technical report, pp. 32, Southampton Oceanogr. Cent., Southampton, U. K.
Neumaier, M., R. Ruhnke, O. Kirner, H. Ziereis, G. Stratmann, C. Brenninkmeijer, and A. Zahn (2014), Impact of acetone (photo)oxidation on HO_x production in the UT/LMS based on CARIBIC passenger aircraft observations and EMAC simulations, *Geophys. Res. Lett.*, *41*, 3289–3297, doi:10.1002/2014GL059480.
Nightingale, P. D., G. Malin, C. S. Law, A. J. Watson, P. S. Liss, M. J. Liddicoat, J. Boutin, and R. C. Upstill-Goddard (2000), In situ evaluation of air-sea gas exchange using novel conservative and volatile tracers, *Global Biogeochem. Cycles*, *14*, 373–387.
Pozzer, A., P. Joeckel, R. Sander, J. Williams, L. Ganzeveld, and J. Lelieveld (2006), Technical note: The MESSy-submodel AIRSEA calculating the air-sea exchange of chemical species, *Atmos. Chem. Phys.*, *6*, 5435–5444, doi:10.5194/acp-6-5435-2006.
Read, K., L. Carpenter, S. Arnold, R. Beale, P. Nightingale, J. Hopkins, A. Lewis, J. Lee, L. Mendes, and J. Pickering (2012), Multiannual observations of acetone, methanol, and acetaldehyde in remote tropical Atlantic air: Implications for atmospheric OVOC budgets and oxidative capacity, *Environ. Sci. Technol.*, *46*(20), 11,028–11,039.
Schade, G. W., and A. H. Goldstein (2006), Seasonal measurements of acetone and methanol: Abundances and implications for atmospheric budgets, *Global Biogeochem. Cycles*, *20*, GB1011, doi:10.1029/2005GB002566.
Singh, H. B., M. Kanakidou, P. J. Crutzen, and D. J. Jacob (1995), High concentrations and photochemical fate of oxygenated hydrocarbons in the global troposphere, *Nature*, *378*, 50–54.
Singh, H. B., et al. (2000), Distribution and fate of selected oxygenated organic species in the troposphere and lower stratosphere over the Atlantic, *J. Geophys. Res.*, *105*, 3795–3805.
Snider, J., and G. Dawson (1985), Tropospheric light alcohols, carbonyls, and acetonitrile: Concentrations in the southwestern United States and Henry's law data, *J. Geophys. Res.*, *90*, 3797–3805.
Sweeney, C., E. Gloor, A. R. Jacobson, R. M. Key, G. McKinley, J. L. Sarmiento, and R. Wanninkhof (2007), Constraining global air-sea gas exchange for CO_2 with recent bomb 14C measurements, *Global Biogeochem. Cycles*, *21*, GB2015, doi:10.1029/2006GB002784.
Veron, F., G. Saxena, and S. K. Misra (2007), Measurements of the viscous tangential stress in the airflow above wind waves, *Geophys. Res. Lett.*, *34*, L19603, doi:10.1029/2007GL031242.
Williams, J., R. Holzinger, V. Gros, X. Xu, E. Atlas, and D. Wallace (2004), Measurements of organic species in air and seawater from the tropical Atlantic, *Geophys. Res. Lett.*, *31*, L23S06, doi:10.1029/2004GL020012.
Woolf, D. K. (1997), Bubbles and their role in gas exchange, in *The Sea Surface and Global Change*, edited by R. Duce and P. Liss, pp. 173–205, Cambridge Univ. Press, N. Y.
Yang, M., B. Blomquist, C. Fairall, S. Archer, and B. Huebert (2011), Air-sea exchange of dimethylsulfide (DMS) in the Southern Ocean—Measurements from SO GasEx compared to temperate and tropical regions, *J. Geophys. Res.*, *116*, C00F05, doi:10.1029/2010JC006526.
Yang, M., R. Beale, T. Smyth, and B. Blomquist (2013a), Measurements of OVOC fluxes by eddy covariance using a proton-transfer-reaction mass spectrometer—Method development at a coastal site, *Atmos. Chem. Phys.*, *13*, 6165–6184, doi:10.5194/acp-13-6165-2013.
Yang, M., P. Nightingale, R. Beale, P. Liss, B. Blomquist, and C. Fairall (2013b), Atmospheric deposition of methanol over the Atlantic Ocean, *Proc. Natl. Acad. Sci. U. S. A.*, *107*, 16,420–16,427.
Yang, M., R. Beale, P. Liss, M. Johnson, B. Blomquist, and P. Nightingale (2014), Air–sea fluxes of oxygenated volatile organic compounds across the Atlantic Ocean, *Atmos. Chem. Phys.*, *14*, 7499–7517, doi:10.5194/acp-14-7499-2014.
Zhou, X., and K. Mopper (1990), Apparent partition coefficients of 15 carbonyl compounds between air and seawater and between air and freshwater; implications for air-sea exchange, *Environ. Sci. Technol.*, *24*, 1864–1869.